Physics Letters B 788 (2019) 166–179

Contents lists available at ScienceDirect

Physics Letters B

www.elsevier.com/locate/physletb

Transverse momentum spectra and nuclear modification factors of charged particles in Xe–Xe collisions at $\sqrt{s_{\rm NN}} = 5.44$ TeV

ALICE Collaboration *

ARTICLE INFO

Article history:
Received 24 May 2018
Received in revised form 26 September 2018
Accepted 24 October 2018
Available online 31 October 2018
Editor: M. Doser

ABSTRACT

Transverse momentum ($p_{\rm T}$) spectra of charged particles at mid-pseudorapidity in Xe–Xe collisions at $\sqrt{s_{\rm NN}} = 5.44$ TeV measured with the ALICE apparatus at the Large Hadron Collider are reported. The kinematic range $0.15 < p_{\rm T} < 50$ GeV/c and $|\eta| < 0.8$ is covered. Results are presented in nine classes of collision centrality in the 0–80% range. For comparison, a pp reference at the collision energy of $\sqrt{s} = 5.44$ TeV is obtained by interpolating between existing pp measurements at $\sqrt{s} = 5.02$ and 7 TeV. The nuclear modification factors in central Xe–Xe collisions and Pb–Pb collisions at a similar center-of-mass energy of $\sqrt{s_{\rm NN}} = 5.02$ TeV, and in addition at 2.76 TeV, at analogous ranges of charged particle multiplicity density $\langle {\rm d}N_{\rm ch}/{\rm d}\eta \rangle$ show a remarkable similarity at $p_{\rm T} > 10$ GeV/c. The centrality dependence of the ratio of the average transverse momentum $\langle p_{\rm T} \rangle$ in Xe–Xe collisions over Pb–Pb collision at $\sqrt{s} = 5.02$ TeV is compared to hydrodynamical model calculations.

1. Introduction

Transverse momentum ($p_{\rm T}$) spectra of charged particles carry essential information about the high-density deconfined state of strongly-interacting matter commonly denoted as quark–gluon plasma, that is formed in high-energy nucleus–nucleus (A–A) collisions [1]. Relativistic hydrodynamics is able to model the evolution of this medium [2,3].

At low to intermediate $p_{\rm T}$, typically in the range of up to 10 GeV/c, charged particle production is governed by the collective expansion of the system, which is observed in the shapes of single-particle transverse-momentum spectra [4,5] and multi-particle correlations [2]. However, there is presently an intense debate as to whether the strikingly similar signatures observed in small collision systems (pp and p–A) are also of hydrodynamical origin [6–14]. A key ingredient of calculations in relativistic hydrodynamics is the initial energy density [2,15,16]. The number of produced particles and the volume of the medium are approximately proportional to the number of nucleons $N_{\rm part}$ that participate in the collision [17–19]. Thus, the particle density per unit volume is roughly independent of $N_{\rm part}$. As a consequence, particle spectra at small transverse momentum should be similar in nucleus–nucleus collisions, independently of the mass number, when compared at similar values of $N_{\rm part}$ [20].

At high $p_{\rm T}$, typically above 10 GeV/c, particles originate from parton fragmentation and are sensitive to the amount of energy loss that the partons suffer when propagating in the medium. In a simplified model, the energy loss depends on the number of scattering centers, which is roughly proportional to the energy density, and on the path length that the parton propagates in the medium [21]. For elastic collisions, the dependence is linear, while for medium induced gluon radiation, it is quadratic [22]. A description of experimental data lies in between those two [23].

For hard processes, the production yield $N_{\rm AA}$ in nucleus–nucleus (A–A) collisions is expected to scale with the average nuclear overlap function $\langle T_{\rm AA} \rangle$ when compared to the production cross section $\sigma_{\rm pp}$ in pp collisions. In the absence of nuclear effects, the nuclear modification factor

$$R_{\rm AA}(p_{\rm T}) = \frac{1}{\langle T_{\rm AA} \rangle} \cdot \frac{{\rm d}N_{\rm AA}(p_{\rm T})/{\rm d}p_{\rm T}}{{\rm d}\sigma_{\rm pp}(p_{\rm T})/{\rm d}p_{\rm T}} \quad (1)$$

equals unity. The average nuclear overlap function is defined as the average number of binary nucleon-nucleon collisions $\langle N_{\rm coll} \rangle$ per inelastic nucleon-nucleon cross section and is estimated via a Glauber model calculation [24]. At the Large Hadron Collider (LHC), particle production is observed to be strongly suppressed in Pb–Pb collisions by a factor of up to 7–8 around $p_{\rm T} = 6$–7 GeV/c with a linear decrease of the suppression factor at higher $p_{\rm T}$ but still a substantial suppression even above 100 GeV/c [5,25].

The LHC produced for the first time collisions of xenon nuclei at a center-of-mass energy of $\sqrt{s_{\rm NN}} = 5.44$ TeV during a pilot run with 6 hours of stable beams in October 2017. This allows for studying the dependence of particle production on the collision system size where xenon neatly bridges the gap between data

* *E-mail address:* alice-publications@cern.ch.

https://doi.org/10.1016/j.physletb.2018.10.052

Table 1
Averaged values of $\langle dN_{ch}/d\eta \rangle$, $\langle N_{part} \rangle$, $\langle N_{coll} \rangle$ and $\langle T_{AA} \rangle$ for nine centrality classes of Xe–Xe collisions [18,19] at $\sqrt{s_{NN}} = 5.44$ TeV, and $\langle dN_{ch}/d\eta \rangle$ for Pb–Pb collisions at $\sqrt{s_{NN}} = 5.02$ TeV [30]. The values for $\langle dN_{ch}/d\eta \rangle$ are measured in the range $|\eta| < 0.5$.

Centrality (%)	$\langle dN_{ch}/d\eta \rangle_{Xe-Xe}$	$\langle N_{part} \rangle$	$\langle N_{coll} \rangle$	$\langle T_{AA} \rangle$ (mb^{-1})	$\langle dN_{ch}/d\eta \rangle_{Pb-Pb}$
0–5	1167 ± 26	236 ± 2	949 ± 53	13.9 ± 0.8	1943 ± 54
5–10	939 ± 24	207 ± 2	737 ± 46	10.8 ± 0.7	1586 ± 46
10–20	706 ± 17	165 ± 2	511 ± 26	7.5 ± 0.5	1180 ± 31
20–30	478 ± 11	118 ± 3	303 ± 28	4.4 ± 0.4	786 ± 20
30–40	315 ± 8	82 ± 3	171 ± 19	2.5 ± 0.3	512 ± 15
40–50	198 ± 5	55 ± 3	92 ± 11	1.3 ± 0.2	318 ± 12
50–60	118 ± 3	34 ± 2	46 ± 6	0.7 ± 0.1	183 ± 8
60–70	65 ± 2	20 ± 2	22 ± 3	0.32 ± 0.04	96 ± 6
70–80	32 ± 1	11 ± 1	10 ± 1	0.14 ± 0.02	45 ± 3

from pp, p–Pb and Pb–Pb collisions. Here, the atomic mass numbers are $A = 129$ for xenon, and $A = 208$ for lead with half-density radii of the nuclear-charge distribution of $r = (5.36 \pm 0.1)$ fm and (6.62 ± 0.06) fm, respectively [24,26]. The parameters of the nuclear-charge density distribution for ^{129}Xe are not yet measured but were extrapolated from neighboring isotopes and are thus less precisely known than for ^{208}Pb. While ^{208}Pb is a spherical nucleus, ^{129}Xe has a deformation parameter of $\beta_2 = (0.18 \pm 0.02)$.

This article reports transverse momentum spectra of charged particles at mid-pseudorapidity in Xe–Xe collisions at $\sqrt{s_{NN}} = 5.44$ TeV measured with the ALICE apparatus at the LHC in the kinematic range $0.15 < p_T < 50$ GeV/c and $|\eta| < 0.8$ for nine classes of collision centrality, covering the most central 80% of the hadronic cross section. It is organized as follows: Section 2 describes the experimental setup and data analysis. Systematic uncertainties are discussed in Sect. 3. Results and comparison to model calculations are presented in Sect. 4. A summary is given in Sect. 5.

2. Experiment and data analysis

Collisions of xenon nuclei were recorded at an average instantaneous luminosity of about $2 \cdot 10^{-25}$ cm^{-2} s^{-1} and a hadronic interaction rate of 80–150 s^{-1}. A detailed description of the ALICE experimental apparatus can be found elsewhere [27].

2.1. Trigger and event selection

A minimum-bias interaction trigger was optimized for high efficiency on hadronic collisions. It required signals from both forward scintillator arrays covering $2.8 < \eta < 5.1$ (V0A) and $-3.7 < \eta < -1.7$ (V0C). Additionally, coincidence with signals from two neutron Zero-Degree Calorimeters (ZDC), ZNA and ZNC, at $|\eta| > 8.7$ was required in order to remove contamination from electromagnetic processes. Here A and C denote opposite sides of the experiment along the beamline. The offline event selection was optimized to reject beam-induced background. Background events were efficiently rejected by exploiting the timing signals in the two V0 detectors. Parasitic collisions are removed by using the correlation between the sum and the difference in arrival times as measured in each of the neutron ZDCs. In total, $1.1 \cdot 10^6$ minimum-bias collisions pass the event selection and were further analyzed.

This analysis is based on tracking information from the Inner Tracking System (ITS) [28] and the Time Projection Chamber (TPC) [29] which are located in the central barrel of ALICE. A solenoidal magnet provides momentum dispersion in the direction transverse to the beam axis. The nominal field strength in the ALICE central barrel is 0.5 T. However, in order to extend particle tracking and identification to the lowest possible momenta, it was reduced to 0.2 T in Xe–Xe collisions.

The ITS is comprised of six cylindrical layers of silicon detectors with radii between 3.9 and 43.0 cm. The two innermost layers, with average radii of 3.9 cm and 7.6 cm, are equipped with Silicon Pixel Detectors (SPD); the two intermediate layers, with average radii of 15.0 cm and 23.9 cm, are equipped with Silicon Drift Detectors (SDD) and the two outermost layers, with average radii of 38.0 cm and 43.0 cm, are equipped with double-sided Silicon Strip Detectors (SSD). The large cylindrical TPC has an active radial range from about 85 to 250 cm and an overall length along the beam direction of 500 cm. It covers the full azimuth in the pseudo-rapidity range $|\eta| < 0.9$ and provides track reconstruction with up to 159 points along the trajectory of a charged particle as well as particle identification via the measurement of specific energy loss dE/dx.

The collision vertex is determined using reconstructed particle trajectories in the TPC including hits in the ITS. All collisions with a reconstructed vertex position within ±10 cm along the beam direction from the nominal interaction point are accepted. The collision centrality is defined as the percentile of the hadronic cross section corresponding to the measured charged particle multiplicity. The centrality determination is based on the sum of the amplitudes of the V0A and V0C signals [18,19]. Averaged quantities characterizing a centrality class such as the number of participants N_{part}, the number of binary collisions N_{coll}, and the nuclear overlap function T_{AA} are calculated as the average over all events in this class by fitting the experimental distribution with a Glauber Monte Carlo model that employs negative binomial distributions to model multiplicity production [18,19] (see Table 1). The analysis is restricted to the 0–80% centrality range in order to ensure that effects of trigger inefficiency and contamination by electromagnetic processes are negligible.

2.2. Track selection

Primary charged particles within the kinematic range $|\eta| < 0.8$ and $0.15 < p_T < 50$ GeV/c are measured. Here, primaries are defined as all charged particles with a proper lifetime τ larger than 1 cm/c that are either produced directly in the primary beam-beam interaction, or from decays of particles with τ smaller than 1 cm/c, excluding particles produced in interactions with the detector material [31]. The track selection is optimized for best track quality and minimum contamination from secondary particles. The selection criteria are identical to those of the previous analysis of Pb–Pb collisions at $\sqrt{s_{NN}} = 5.02$ TeV [5] except for the following changes in the parameterization on the transverse momentum dependence. The geometrical track length in the TPC fiducial volume [29] is $L/(1\,\text{cm}) > 130 - (p_T/(1\ \text{GeV}/c))^{-0.7}$, and the distance of closest approach to the primary vertex in the transverse plane is $|\text{DCA}_{xy}|/(1\,\text{cm}) < 0.0119 + 0.049\,(p_T/(1\ \text{GeV}/c))^{-1}$. These changes reflect differences in particle tracking due to the reduced magnetic field. In order to reject fake tracks that contaminate the spectrum, especially at high p_T, another selection is introduced: the uncertainty in the reconstructed p_T as estimated from the covariance

matrix of the track fit must be less than ten times the standard deviation, when averaged over all tracks at that momentum.

2.3. Corrections

The doubly-differential transverse momentum spectra in Xe–Xe collisions are normalized by the number of events $N_{\rm ev}$ in each centrality class, and are given by

$$\frac{1}{N_{\rm ev}}\frac{{\rm d}^2N_{\rm ch}}{{\rm d}\eta{\rm d}p_{\rm T}} \equiv \frac{N_{\rm ch}^{\rm rec}(\Delta\eta,\Delta p_{\rm T})}{N_{\rm ev}\cdot\Delta\eta\Delta p_{\rm T}}\cdot\frac{\delta_{p_{\rm T}}(\Delta p_{\rm T})}{\alpha(\Delta p_{\rm T})\cdot\varepsilon(\Delta p_{\rm T})}, \quad (2)$$

where $N_{\rm ch}^{\rm rec}$ is the raw yield of reconstructed primary charged particles in each interval of pseudo-rapidity and transverse momentum $(\Delta\eta,\Delta p_{\rm T})$. The symbols $\alpha(\Delta p_{\rm T})$ and $\varepsilon(\Delta p_{\rm T})$ are the correction factors for detector acceptance and tracking efficiency, respectively. The correction due to the finite transverse-momentum resolution in the reconstruction of primary charged particles is denoted by $\delta_{p_{\rm T}}(\Delta p_{\rm T})$. The efficiencies for trigger, event vertex reconstruction and tracking are estimated using Monte Carlo simulations with HIJING [32] as the event generator and GEANT3 [33] for particle propagation and simulation of the detector response. The trigger and vertex selections are fully efficient for the whole centrality range used in the analysis.

Contamination from secondary charged particles, i.e. from weak decays and interactions in the detector material, is subtracted from the raw spectrum by employing a data driven method [5]. Reconstructed trajectories of primary charged particles point to the collision vertex, while charged particles from weak decays and particles generated in the detector material preferentially point away from it. In order to distinguish between primary and secondary particles, the distance of closest approach to the collision vertex in radial direction, $\rm DCA_{xy}$, is used. A multi-template function that consists of templates for primary particles, secondary particles produced from weak decays and secondary particles from interactions in the detector material is fitted to the $\rm DCA_{xy}$ distributions in each $p_{\rm T}$ interval.

The primary charged particle reconstruction efficiency is obtained from the Monte Carlo simulation. As discussed in detail in [5], this efficiency depends on the relative abundances of the various primary particles species. These relative abundances are adjusted in the simulation using a data-driven re-weighting procedure. The particle composition in Xe–Xe collisions is not yet known. However, bulk particle production scales with the average charged particle multiplicity density, $\langle {\rm d}N_{\rm ch}/{\rm d}\eta\rangle$, independently of the collision system [34]. In Xe–Xe collisions, the weights from existing analyses [35–37,4,5] with Pb–Pb collisions at $\sqrt{s_{\rm NN}} = 2.76$ TeV at equivalent values in $\langle {\rm d}N_{\rm ch}/{\rm d}\eta\rangle$ are applied.

The acceptance times tracking efficiency for charged pions, charged kaons and (anti-)protons for 5% most central Xe–Xe collisions is shown in Fig. 1 as a function of the particle transverse momentum and compared to 10–20% Pb–Pb collisions at $\sqrt{s_{\rm NN}} = 5.02$ TeV. The two centrality classes have similar multiplicity densities. The particular shape with a dip at $p_{\rm T}\sim 0.4$ GeV/c arises from the geometrical length selection that is especially visible for pions. This dip corresponds to particles that cross the TPC sector boundaries under small angles. The decrease at low values of $p_{\rm T}$ is due to curling trajectories in the magnetic field which do not reach the required minimum track length in the TPC and due to energy loss and absorption in the detector material. In Pb–Pb collisions, the magnetic field was set to $B = 0.5$ T, which results in the dip being positioned around 1 GeV/c. At large $p_{\rm T}$, above 7 GeV/c, the tracking efficiency is reduced by an increased local track density, i.e. high $p_{\rm T}$ particles are preferentially produced within jets, leading to a slight decrease in the track finding performance.

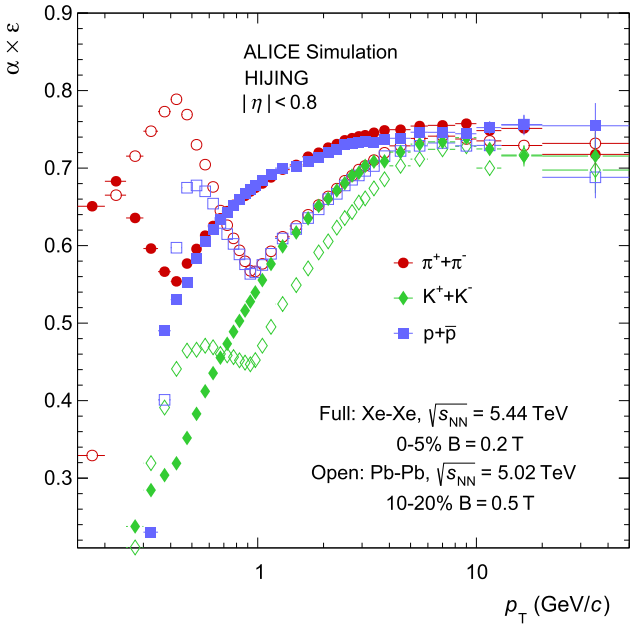

Fig. 1. Transverse momentum dependence of the acceptance times tracking efficiency for the 5% most central Xe–Xe collisions and comparison to the 10–20% centrality class for Pb–Pb collisions. The two centrality classes have similar multiplicity densities.

The transverse momentum of primary charged particles is reconstructed from the track curvature as measured by the ITS and the TPC [38]. The finite momentum resolution modifies the reconstructed charged-particle spectrum and is estimated by the corresponding covariance matrix element of the Kalman fit. The relative $p_{\rm T}$ resolution, $\sigma(p_{\rm T})/p_{\rm T}$, depends on the momentum and amounts to approximately 4.5% at $p_{\rm T} = 0.15$ GeV/c, it shows a minimum of 1.5% around $p_{\rm T} = 1.0$ GeV/c, and increases linearly for larger $p_{\rm T}$, approaching 9.3% at 50 GeV/c. The centrality dependence of the relative $p_{\rm T}$ resolution is negligible. To account for the finite $p_{\rm T}$ resolution, correction factors to the spectra are determined from an unfolding procedure as described in [5], using Bayesian unfolding at low $p_{\rm T}$ and a bin-by-bin correction at large $p_{\rm T}$. The $p_{\rm T}$ dependent correction factors are applied to the measured $p_{\rm T}$ spectrum and depend slightly on collision centrality because of the change in the slope of the spectrum at high $p_{\rm T}$. At transverse momenta below 10 GeV/c, $\delta_{p_{\rm T}}$ deviates significantly from unity only at the lowest momentum interval of $0.15 \le p_{\rm T} < 0.2$ GeV/c where it amounts to 0.5% for all centrality classes, and by up to 3% (4%) in 0–5% (70–80%) central collisions above 10 GeV/c.

The statistical uncertainty of the spectra is dominated by the statistical uncertainty in the raw data. It is largest at the highest momentum interval of 40–50 GeV/c and amounts to 28% (38%) for the 0–5% (30–40%) centrality class while the contribution from the Monte Carlo efficiency is 2% (4%) or less.

2.4. pp reference at $\sqrt{s} = 5.44$ TeV

The $p_{\rm T}$-differential inelastic cross section in pp collisions at $\sqrt{s} = 5.44$ TeV is needed to measure the corresponding nuclear modification factor. As there are no measurements of pp collisions at this energy, a reference is obtained by interpolating pp references as measured at $\sqrt{s} = 5.02$ TeV and $\sqrt{s} = 7$ TeV assuming a power-law dependence in each $p_{\rm T}$ interval, $d\sigma/dp_{\rm T}(\sqrt{s}) \propto \sqrt{s}^{n}$. The value of the free parameter n varies between 0.35 and 1.75, depending on $p_{\rm T}$. This approach is a combination of the interpolation method that was used over the full $p_{\rm T}$ range in [6] and for

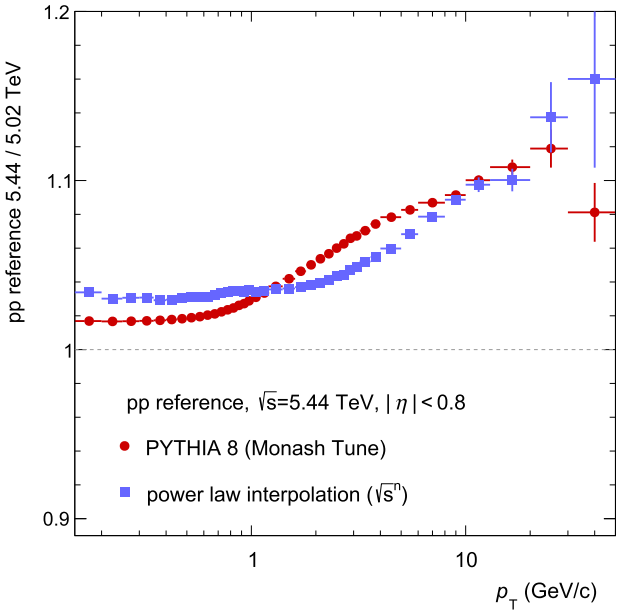

Fig. 2. Ratio of p_{T}-differential inelastic cross sections in pp collisions at $\sqrt{s} = 5.44$ TeV over 5.02 TeV using a power law interpolation and the event generator PYTHIA 8.

$p_{\mathrm{T}} < 5$ GeV/c as used in [39]. The statistical uncertainty of the pp reference is interpolated between the references at $\sqrt{s} = 5.02$ TeV and 7 TeV assuming also a power-law dependence and is assigned to the interpolated reference. It amounts to 7.8% at the momentum interval of 30–50 GeV/c.

As an alternative approach, the scaling of the measured cross section at $\sqrt{s} = 5.02$ TeV to $\sqrt{s} = 5.44$ TeV by using the ratio of spectra at those two energies obtained with the PYTHIA 8 (Monash tune) event generator [40] is studied. The ratio of the pp references at $\sqrt{s} = 5.44$ TeV from the power-law interpolation and at $\sqrt{s} = 5.02$ TeV is shown in Fig. 2 together with results obtained with the alternative method. The spectrum is harder at higher collision energy, with a small change in the total cross section of 4% below 1 GeV/c and an increase of about 10% at transverse momenta above 10 GeV/c.

3. Systematic uncertainties

For the total systematic uncertainty, all contributions are added in quadrature and are summarized in Table 2.

The effect of the selection of events based on the vertex position is studied by comparing the fully corrected p_{T} spectra obtained with alternative vertex selections corresponding to ±5 cm, and ±20 cm. The difference in the fully corrected p_{T} spectra is less than 0.3% for central collisions and less than 0.5% for peripheral collisions.

In order to test the description of the detector response and the track reconstruction in the simulation, all criteria for track selection are varied within the ranges as described in the previous publication [5]. A full analysis is performed by varying one selection criterion at a time. The maximum change in the corrected p_{T} spectrum is then considered as systematic uncertainty. The overall systematic uncertainty related to track selection is obtained from summing up all individual contributions quadratically and it amounts to 0.6–3.0%, depending on p_{T} and centrality.

The systematic uncertainty on the secondary-particle contamination is estimated by varying the fit model using two templates, i.e. for primaries and secondaries, or three templates, i.e. primaries, secondaries from interactions in the detector material and secondaries from weak decays of $\mathrm{K}^0_{\mathrm{S}}$ and Λ, as well as varying the fit ranges. The maximum difference between data and the two-component-template fit is summed in quadrature together with the difference between results obtained from the two- and three-component-template fits. The systematic uncertainty due to the contamination from secondaries is decreasing with increasing p_{T}. It dominates at low p_{T} with values up to 4% and is negligible above 2 GeV/c.

The systematic uncertainty on the primary particle composition is taken from [5]. An additional uncertainty is estimated by assuming the particle composition from a neighboring $\langle \mathrm{d}N_{\mathrm{ch}}/\mathrm{d}\eta \rangle$ range to the matched one in the Pb–Pb analysis and is added quadratically. The sum peaks around 3 GeV/c with a maximum of 5% (less than 2%) for the 0–5% (70–80%) centrality class.

In order to estimate the systematic uncertainty due to the tracking efficiency, the track matching between the TPC and the ITS information in data and Monte Carlo is compared after scaling the fraction of secondary particles obtained from the fits to the $\mathrm{DCA}_{\mathrm{xy}}$ distributions [5]. The difference in the TPC-ITS track-matching efficiency between data and simulation is assigned to the corresponding systematic uncertainty (see Table 2). It amounts to 2% in central collisions, and up to 3.5% in peripheral collisions.

The material budget in ALICE at $\eta \approx 0$ amounts to (11.4 ± 0.5)% in radiation lengths for primary charged particles that have sufficient track length in the TPC [38]. A difference in the amount of detector material leads to different amounts of secondary particles that are produced. After the subtraction of the contribution due to secondaries using the three-component $\mathrm{DCA}_{\mathrm{xy}}$ fits, the differences on the secondary correction factor is negligible. A variation of the material budget within above limits leads to a p_{T} dependent systematic uncertainty on the tracking efficiency of 0.1–0.3%.

The uncertainty due to the finite p_{T} resolution at high p_{T} is estimated using the azimuthal dependence of the $1/p_{\mathrm{T}}$ spectra for

Table 2
Contributions to the systematic uncertainty in units of percent for the 0–5%, 30–40%, and 70–80% centrality classes in Xe–Xe collisions. The numbers are averaged in the p_{T} intervals from 0.2–0.5 GeV/c (left), 1–2 GeV/c (middle) and 40–50 GeV/c (right). For the p_{T}-dependent sum, contributions are added in quadrature.

Centrality (%)	0–5 (%)	30–40 (%)	70–80 (%)
p_{T} range (GeV/c)	0.2–0.5/1–2/40–50	0.2–0.5/1–2/40–50	0.2–0.5/1–2/40–50
Source			
Vertex selection	0.2/0.2/0.2	0.8/0.8/0.8	0.8/0.8/0.8
Track selection	1.6/0.9/1.2	0.9/0.6/0.8	0.9/0.5/1.0
Secondary particles	1.4/0.2/negl.	0.8/0.2/negl.	0.6/0.2/negl.
Particle composition	0.3/1.7/0.7	0.4/1.9/1.0	0.7/0.6/0.6
Tracking efficiency	1.9/1.2/0.4	2.2/1.2/0.4	2.2/1.4/0.6
Material budget	0.3/0.3/0.1	0.3/0.3/0.1	0.3/0.3/0.1
p_{T} resolution	negl./negl./0.5	negl./negl./0.7	negl./negl./0.9
Sum, p_{T} dependent:	3.1/2.4/1.5	2.8/2.5/1.8	2.8/1.9/2.1
Centrality selection	0.1	0.8	3.2

positively and negatively charged particles. The relative shift of the spectra for oppositely charged particles along $1/p_{\mathrm{T}}$ determines the size of uncertainty for a given angle. The RMS of the $1/p_{\mathrm{T}}$ shift as distributed over the full azimuth is used as an additional increase of the p_{T} resolution. For the lowest p_{T} bin the uncertainty is estimated from the unfolding procedure applied to Monte Carlo simulations. The uncertainty due to the finite p_{T} resolution is significant only at the lowest and highest momenta bins and amounts to 0.5% at the lowst p_{T} bin for all centralities and 0.5% (0.9%) for the 0–5% (70–80%) centrality class.

The uncertainty due to the centrality determination is estimated by changing the fraction of the visible cross section (90.0 ± 0.5)%. The uncertainty is estimated from the variation of the resulting p_{T} spectra and amounts to ∼0.1% and ∼3.2% for central (0–5%) and peripheral (70–80%) collisions, respectively.

The systematic uncertainty of the pp reference at $\sqrt{s} = 5.44$ TeV has two contributions, which are added quadratically. For each p_{T} interval, the systematic uncertainty of the pp references at $\sqrt{s} = 5.02$ TeV and $\sqrt{s} = 7$ TeV are interpolated to $\sqrt{s} = 5.44$ TeV by using a power-law. This corresponds to interpolating between the upper and lower boundaries of the experimental data points as given by their systematic uncertainties. It assumes full correlation of systematic uncertainties at both energies.

The difference between the interpolated reference and the one using the PYTHIA 8 event generator is assigned as the other contribution to the systematic uncertainty in the pp reference, in each p_{T} interval. The systematic uncertainty in the pp reference has a minimum of 2.2% around 1 GeV/c and reaches its maximum of 7.7% at the highest momentum bin.

4. Results

The transverse momentum spectra of charged particles in Xe–Xe collisions are shown in the top panel of Fig. 3 for nine centrality classes together with the interpolated pp reference spectrum at $\sqrt{s} = 5.44$ TeV. The latter is obtained from the interpolated p_{T}-differential cross section by dividing it by the interpolated inelastic nucleon-nucleon cross section of (68.4 ± 0.5) mb at $\sqrt{s} = 5.44$ TeV [24]. In the most-peripheral collisions, the p_{T} spectrum is similar to that of pp collisions and exhibits a power law behavior that is characteristic of hard-parton scattering and vacuum fragmentation. With increasing collision centrality, the p_{T} differential cross section is progressively depleted above 5 GeV/c.

Systematic uncertainties are shown in the bottom panel. At momenta between 0.4 and 10 GeV/c, the systematic uncertainty is dominated by the contribution from tracking and amounts to about 2–3%. It is almost independent of p_{T} above 10 GeV/c with a value of 1.4% (2.1%) for the 0–5% (70–80%) centrality class.

In order to determine the nuclear modification factor R_{AA}, the interpolated p_{T}-differential pp cross section is scaled by the average nuclear overlap function $\langle T_{\mathrm{AA}} \rangle$. The resulting nuclear modification factor as a function of transverse momentum is shown in Fig. 4 for nine centrality classes and compared to results from Pb–Pb collisions [5]. The overall normalization uncertainties for R_{AA} are indicated by vertical bars around unity. The uncertainties of the pp reference and the centrality determination are added in quadrature. The latter is larger for Xe–Xe collisions than for Pb–Pb because of the less precisely known nuclear-charge-density distribution of the deformed ^{129}Xe and the resulting larger relative uncertainty in $\langle T_{\mathrm{AA}} \rangle$ [18,19]. The nuclear modification factor exhibits a strong centrality dependence with a minimum around $p_{\mathrm{T}} = 6$–7 GeV/c and an almost linear rise above. In particular, in the 5% most central Xe–Xe collisions, at the minimum, the yield is suppressed by a factor of about 6 with respect to the scaled pp reference. The nuclear modification factor reaches a value of

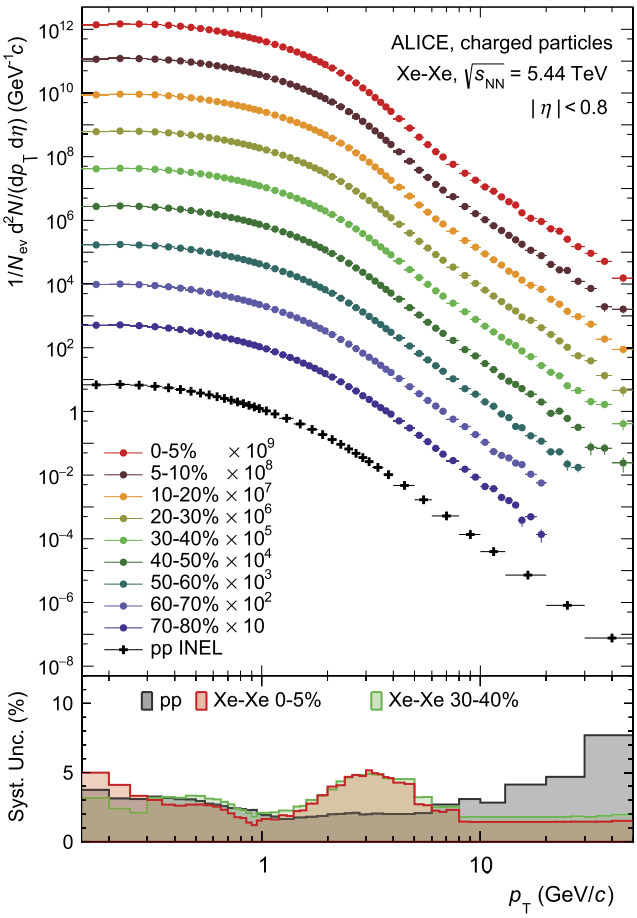

Fig. 3. Transverse momentum spectra of charged particles in Xe–Xe collisions at $\sqrt{s_{\mathrm{NN}}} = 5.44$ TeV in nine centrality classes together with the interpolated pp reference spectrum at $\sqrt{s} = 5.44$ TeV (top panel) and systematic uncertainties (bottom panel).

0.6 at the highest measured transverse-momentum interval of 30–50 GeV/c. For comparison, the nuclear modification factor R_{AA} in Pb–Pb collisions at $\sqrt{s_{\mathrm{NN}}} = 5.02$ TeV is shown in Fig. 4 as open circles for the same centrality classes as Xe–Xe. In both collision systems, a similar characteristic p_{T} dependence of R_{AA} is observed. In Pb–Pb collisions, the suppression of high-momentum particles is apparently stronger for the same centrality class but still in agreement with Xe–Xe collisions within uncertainties.

Nuclear modification factors from Xe–Xe and Pb–Pb collisions and their ratios at similar ranges of $\langle \mathrm{d}N_{\mathrm{ch}}/\mathrm{d}\eta \rangle$ are shown in Fig. 5. In 5% most central Xe–Xe collisions, the nuclear modification factor is remarkably well matched by 10–20% central Pb–Pb collisions over the entire p_{T} range. In the 30–40% Xe–Xe (40–50% Pb–Pb) centrality class, again agreement is found within uncertainties.These findings of matching nuclear modification factors at similar ranges of $\langle \mathrm{d}N_{\mathrm{ch}}/\mathrm{d}\eta \rangle$ are in agreement with results from the study of fractional momentum loss of high-p_{T} partons at RHIC and LHC energies [41].

A comparison of the nuclear modification factors as a function of $\langle \mathrm{d}N_{\mathrm{ch}}/\mathrm{d}\eta \rangle$ in Xe–Xe and Pb–Pb collisions for three different regions of p_{T} (low, medium, and high) is shown in Fig. 6. A remarkable similarity in R_{AA} is observed between Xe–Xe collision at $\sqrt{s_{\mathrm{NN}}} = 5.44$ TeV and Pb–Pb collisions at $\sqrt{s_{\mathrm{NN}}} = 5.02$ and 2.76 TeV when compared at identical ranges in $\langle \mathrm{d}N_{\mathrm{ch}}/\mathrm{d}\eta \rangle$, for $\langle \mathrm{d}N_{\mathrm{ch}}/\mathrm{d}\eta \rangle > 400$. This holds both at low momentum where the hydrodynamical expansion of the medium dominates the spectrum and at high momentum, where parton energy loss inside the

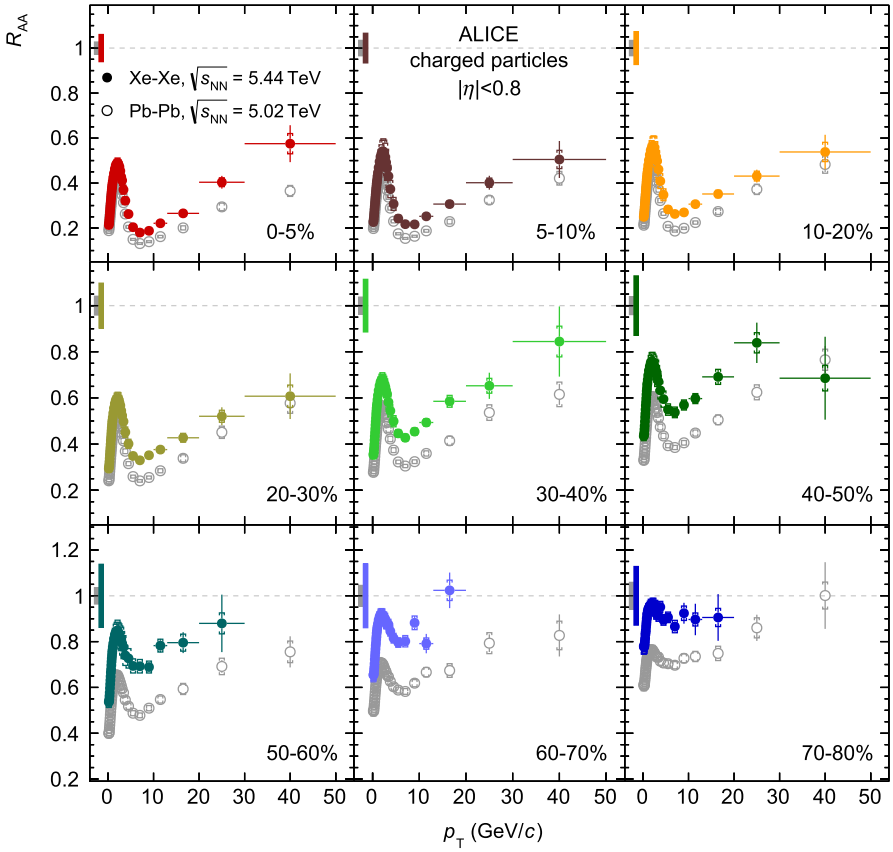

Fig. 4. Nuclear modification factor in Xe–Xe at $\sqrt{s_{NN}} = 5.44$ TeV (filled circles) and Pb–Pb collisions [5] at $\sqrt{s_{NN}} = 5.02$ TeV (open circles) for nine centrality classes. The vertical lines (brackets) represent the statistical (systematic) uncertainties. The overall normalization uncertainty is shown as a filled box around unity.

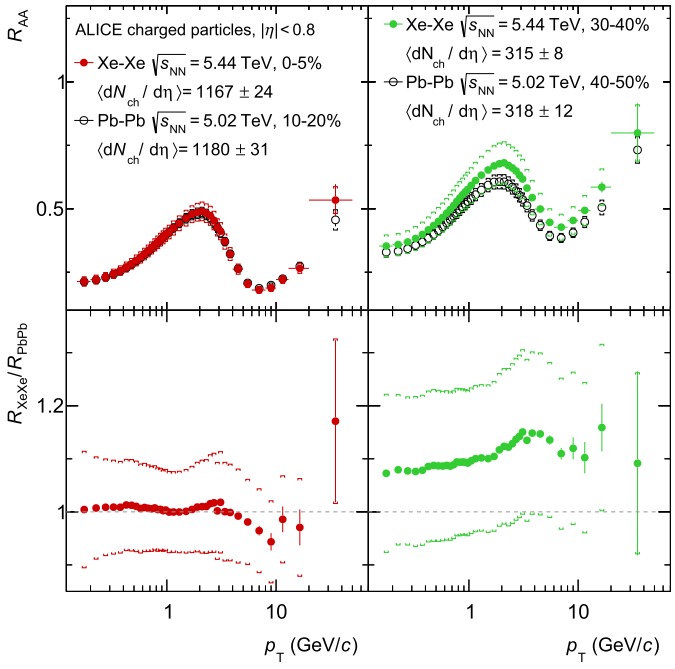

Fig. 5. Comparison of nuclear modification factors in Xe–Xe collisions (filled circles) and Pb–Pb collisions (open circles) for similar ranges in $\langle dN_{ch}/d\eta \rangle$ for the 0–5% (left) and 30–40% (right) Xe–Xe centrality classes. The vertical lines (brackets) represent the statistical (systematic) uncertainties.

medium drives the spectral shape. At $\langle dN_{ch}/d\eta \rangle < 400$, the values of R_{AA} still agree within rather large uncertainties although no definitive conclusion can be drawn because, in particular, event selection and geometry biases could affect the spectrum in peripheral A–A collisions [42].

In a simplified radiative energy loss scenario when assuming identical thermalization times [43,44], the average energy loss $\langle \Delta E \rangle$ is proportional to the density of scattering centers in the medium, which in turn is proportional to the energy density ε, and to the square of the path length L of the parton in the medium, $\langle \Delta E \rangle \propto \varepsilon \cdot L^2$ [22]. The energy density can be estimated from the average charged-particle multiplicity density [45] per transverse area, $\varepsilon \propto \langle dN_{ch}/d\eta \rangle / A_T$. In central collisions, the initial transverse area A_T is related to the radius r of the colliding nuclei, $A_T = \pi \cdot r^2$ [22]. Therefore, the comparison of the measured R_{AA} values in the two colliding systems could enable a test of the path length dependence of medium-induced parton energy loss [46].

To further address bulk production, the average transverse momentum $\langle p_T \rangle$ in the range from 0–10 GeV/c is derived. The spectra are extrapolated down to $p_T = 0$ by fitting a Hagedorn function [47] in the range 0.15 GeV/c < p_T < 1 GeV/c. The relative fraction of the extrapolated particle yield amounts to 8% (11%) for the 0–5% (70–80%) centrality class. Statistical uncertainties in $\langle p_T \rangle$ are negligible. Systematic uncertainties are estimated by varying each source of systematic uncertainty in the spectra at a time, by varying the fit range to 0.15 GeV/c < p_T < 0.5 GeV/c, and by changing the interpolation range to 0–0.2 GeV/c. All contributions are then added quadratically. The relative systematic uncertainty is 1.8% (1.3%) for the 0–5% (70–80%) centrality class.

The average transverse momentum is presented in the top panel of Fig. 7 for Xe–Xe collisions at $\sqrt{s} = 5.44$ TeV (squares) and Pb–Pb collisions at $\sqrt{s} = 5.02$ TeV (diamonds) for nine centrality classes. An increase of $\langle p_T \rangle$ with centrality is visible in both col-

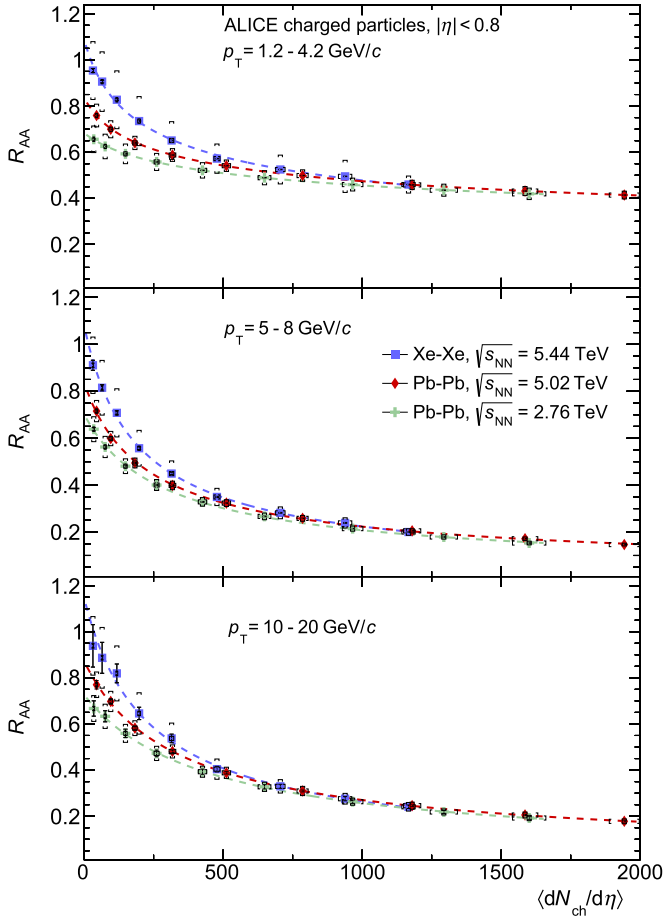

Fig. 6. Comparison of the nuclear modification factor in Xe–Xe and Pb–Pb collisions integrated over identical regions in p_{T} as a function of $\langle \mathrm{d}N_{\mathrm{ch}}/\mathrm{d}\eta \rangle$. The vertical brackets indicate the quadratic sum of the total systematic uncertainty in the measurement and the overall normalization uncertainty in $\langle T_{\mathrm{AA}} \rangle$. The horizontal bars reflect the RMS of the distribution in each bin. The dashed lines show results from power-law fits to the data and are drawn to guide the eye.

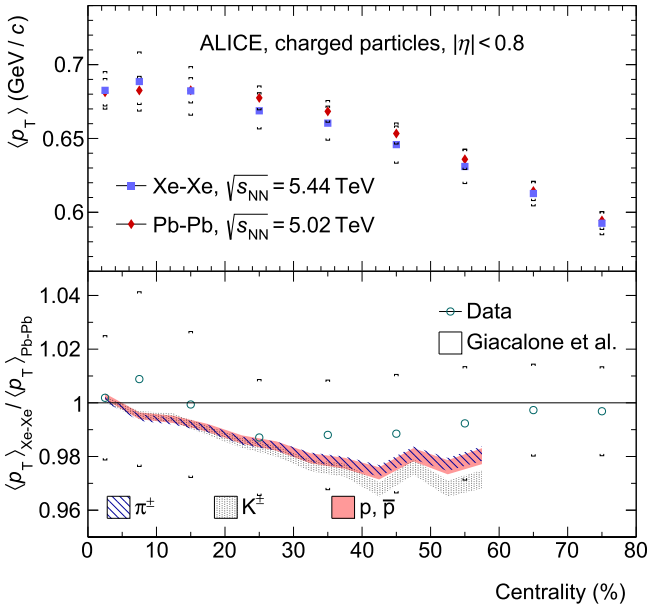

Fig. 7. Average transverse momentum in the p_{T}-range 0–10 GeV/c for Xe–Xe collisions at $\sqrt{s} = 5.44$ TeV (squares) and Pb–Pb collisions at $\sqrt{s} = 5.02$ TeV (diamonds) for nine centrality classes (top) and their ratios (bottom). The vertical brackets indicate systematic uncertainties. The hashed areas show results from hydrodynamical calculations by Giacalone et al. [43].

lision systems and is attributed to the increasing transverse radial flow. The bottom panel of Fig. 7 shows the ratios of $\langle p_{\mathrm{T}} \rangle$ in both collision systems. The ratio is flat within uncertainties but allows for relative variations of up to two percent. Comparison to results from hydrodynamical calculations [43] are shown by the hashed areas for pions, kaons and protons. While the calculations are not able to predict absolute particle spectra, predictions are made for the relative difference in $\langle p_{\mathrm{T}} \rangle$ between both collision systems in order to study the system size dependence. The predicted trend of a larger $\langle p_{\mathrm{T}} \rangle$ in 5% most central Xe–Xe collision and continuously lower values towards the 40–50% centrality class are consistent with the data.

5. Summary

Transverse momentum spectra and nuclear modification factors of charged particles in Xe–Xe collisions at $\sqrt{s_{\mathrm{NN}}} = 5.44$ TeV in the kinematic range $0.15 < p_{\mathrm{T}} < 50$ GeV/c and $|\eta| < 0.8$ are reported for nine centrality classes, in the 0–80% range. A pp reference at $\sqrt{s} = 5.44$ TeV is obtained by the interpolation of the existing spectra at $\sqrt{s} = 5.02$ and 7 TeV. When comparing nuclear modification factors at similar ranges of averaged charged particle multiplicity densities, a remarkable similarity between central Xe–Xe collisions and Pb–Pb collisions at a similar center-of-mass energy of $\sqrt{s_{\mathrm{NN}}} = 5.02$ TeV and at 2.76 TeV is observed for $\langle \mathrm{d}N_{\mathrm{ch}}/\mathrm{d}\eta \rangle > 400$. The centrality dependence of the ratio of the average transverse momentum $\langle p_{\mathrm{T}} \rangle$ in Xe–Xe collisions over Pb–Pb collisions is flat within uncertainties but allows for relative variations of up to two percent. Predictions from hydrodynamical calculations that take into account the significantly different geometries of both collision systems are consistent with the data.

Acknowledgements

The ALICE collaboration would like to thank G. Giacalone, J. Noronha-Hostler, M. Luzum, and J.-Y. Ollitrault for providing the results of their hydrodynamical calculations prior to publication.

The ALICE Collaboration would like to thank all its engineers and technicians for their invaluable contributions to the construction of the experiment and the CERN accelerator teams for the outstanding performance of the LHC complex. The ALICE Collaboration gratefully acknowledges the resources and support provided by all Grid centres and the Worldwide LHC Computing Grid (WLCG) collaboration. The ALICE Collaboration acknowledges the following funding agencies for their support in building and running the ALICE detector: A. I. Alikhanyan National Science Laboratory (Yerevan Physics Institute) Foundation (ANSL), State Committee of Science and World Federation of Scientists (WFS), Armenia; Austrian Academy of Sciences and Nationalstiftung für Forschung, Technologie und Entwicklung, Austria; Ministry of Communications and High Technologies, National Nuclear Research Center, Azerbaijan; Conselho Nacional de Desenvolvimento Científico e Tecnológico (CNPq), Universidade Federal do Rio Grande do Sul (UFRGS), Financiadora de Estudos e Projetos (Finep) and Fundação de Amparo à Pesquisa do Estado de São Paulo (FAPESP), Brazil; Ministry of Science & Technology of China (MSTC), National Natural Science Foundation of China (NSFC) and Ministry of Education of China (MOEC), China; Ministry of Science and Education, Croatia; Ministry of Education, Youth and Sports of the Czech Republic, Czech Republic; The Danish Council for Independent Research | Natural Sciences, the Carlsberg Foundation and Danish National Research Foundation (DNRF), Denmark; Helsinki Institute of Physics

(HIP), Finland; Commissariat à l'Energie Atomique (CEA) and Institut National de Physique Nucléaire et de Physique des Particules (IN2P3) and Centre National de la Recherche Scientifique (CNRS), France; Bundesministerium für Bildung, Wissenschaft, Forschung und Technologie (BMBF) and GSI Helmholtzzentrum für Schwerionenforschung GmbH, Germany; General Secretariat for Research and Technology, Ministry of Education, Research and Religions, Greece; National Research, Development and Innovation Office, Hungary; Department of Atomic Energy, Government of India (DAE), Department of Science and Technology, Government of India (DST), University Grants Commission, Government of India (UGC) and Council of Scientific and Industrial Research (CSIR), India; Indonesian Institute of Science, Indonesia; Centro Fermi - Museo Storico della Fisica e Centro Studi e Ricerche Enrico Fermi and Istituto Nazionale di Fisica Nucleare (INFN), Italy; Institute for Innovative Science and Technology, Nagasaki Institute of Applied Science (IIST), Japan Society for the Promotion of Science (JSPS) KAKENHI and Japanese Ministry of Education, Culture, Sports, Science and Technology (MEXT), Japan; Consejo Nacional de Ciencia (CONACYT) y Tecnología, through Fondo de Cooperación Internacional en Ciencia y Tecnología (FONCICYT) and Dirección General de Asuntos del Personal Academico (DGAPA), Mexico; Nederlandse Organisatie voor Wetenschappelijk Onderzoek (NWO), Netherlands; The Research Council of Norway, Norway; Commission on Science and Technology for Sustainable Development in the South (COMSATS), Pakistan; Pontificia Universidad Católica del Perú, Peru; Ministry of Science and Higher Education and National Science Centre, Poland; Korea Institute of Science and Technology Information and National Research Foundation of Korea (NRF), Republic of Korea; Ministry of Education and Scientific Research, Institute of Atomic Physics and Romanian National Agency for Science, Technology and Innovation, Romania; Joint Institute for Nuclear Research (JINR), Ministry of Education and Science of the Russian Federation and National Research Centre Kurchatov Institute, Russia; Ministry of Education, Science, Research and Sport of the Slovak Republic, Slovakia; National Research Foundation of South Africa, South Africa; Centro de Aplicaciones Tecnológicas y Desarrollo Nuclear (CEADEN), Cubaenergía, Cuba and Centro de Investigaciones Energéticas, Medioambientales y Tecnológicas (CIEMAT), Spain; Swedish Research Council (VR) and Knut & Alice Wallenberg Foundation (KAW), Sweden; European Organization for Nuclear Research, Switzerland; National Science and Technology Development Agency (NSDTA), Suranaree University of Technology (SUT) and Office of the Higher Education Commission under NRU project of Thailand, Thailand; Turkish Atomic Energy Agency (TAEK), Turkey; National Academy of Sciences of Ukraine, Ukraine; Science and Technology Facilities Council (STFC), United Kingdom; National Science Foundation of the United States of America (NSF) and U.S. Department of Energy, Office of Nuclear Physics (DOE NP), United States of America.

References

[1] B. Muller, J. Schukraft, B. Wyslouch, First results from Pb + Pb collisions at the LHC, Annu. Rev. Nucl. Part. Sci. 62 (2012) 361–386, arXiv:1202.3233 [hep-ex].

[2] U. Heinz, R. Snellings, Collective flow and viscosity in relativistic heavy-ion collisions, Annu. Rev. Nucl. Part. Sci. 63 (2013) 123–151, arXiv:1301.2826 [nucl-th].

[3] J.E. Bernhard, J.S. Moreland, S.A. Bass, J. Liu, U. Heinz, Applying Bayesian parameter estimation to relativistic heavy-ion collisions: simultaneous characterization of the initial state and quark–gluon plasma medium, Phys. Rev. C 94 (2) (2016) 024907, arXiv:1605.03954 [nucl-th].

[4] ALICE Collaboration, J. Adam, et al., Centrality dependence of the nuclear modification factor of charged pions, kaons, and protons in Pb–Pb collisions at $\sqrt{s_{\rm NN}} = 2.76$ TeV, Phys. Rev. C 93 (2016) 034913, arXiv:1506.07287 [nucl-ex].

[5] ALICE Collaboration, S. Acharya, et al., Transverse momentum spectra and nuclear modification factors of charged particles in pp, p–Pb and Pb–Pb collisions at the LHC, arXiv:1802.09145 [nucl-ex].

[6] ALICE Collaboration, J. Adam, et al., Multiplicity dependence of charged pion, kaon, and (anti)proton production at large transverse momentum in p–Pb collisions at $\sqrt{s_{\rm NN}} = 5.02$ TeV, Phys. Lett. B 760 (2016) 720–735, arXiv:1601.03658 [nucl-ex].

[7] A. Ortiz, P. Christiansen, E. Cuautle, I. Maldonado, G. Paic, Color reconnection and flow-like patterns in pp collisions, Phys. Rev. Lett. 111 (4) (2013) 042001, arXiv:1303.6326 [hep-ph].

[8] ALICE Collaboration, B.B. Abelev, et al., Long-range angular correlations of pi, K and p in p–Pb collisions at $\sqrt{s_{\rm NN}} = 5.02$ TeV, Phys. Lett. B 726 (2013) 164–177, arXiv:1307.3237 [nucl-ex].

[9] CMS Collaboration, V. Khachatryan, et al., Long-range two-particle correlations of strange hadrons with charged particles in p–Pb and Pb–Pb collisions at LHC energies, Phys. Lett. B 742 (2015) 200–224, arXiv:1409.3392 [nucl-ex].

[10] CMS Collaboration, S. Chatrchyan, et al., Multiplicity and transverse-momentum dependence of two- and four-particle correlations in p–Pb and Pb–Pb collisions, Phys. Lett. B 724 (2013) 213–240, arXiv:1305.0609 [nucl-ex].

[11] CMS Collaboration, V. Khachatryan, et al., Evidence for collective multiparticle correlations in p–Pb collisions, Phys. Rev. Lett. 115 (1) (2015) 012301, arXiv:1502.05382 [nucl-ex].

[12] ATLAS Collaboration, G. Aad, et al., Measurement with the ATLAS detector of multi-particle azimuthal correlations in p + Pb collisions at $\sqrt{s_{\rm NN}} = 5.02$ TeV, Phys. Lett. B 725 (2013) 60–78, arXiv:1303.2084 [hep-ex].

[13] K. Dusling, R. Venugopalan, Comparison of the color glass condensate to dihadron correlations in proton–proton and proton–nucleus collisions, Phys. Rev. D 87 (2013) 094034, arXiv:1302.7018 [hep-ph].

[14] B. Blok, C.D. Jakel, M. Strikman, U.A. Wiedemann, Collectivity from interference, J. High Energy Phys. 12 (2017) 074, arXiv:1708.08241 [hep-ph].

[15] PHENIX Collaboration, A. Adare, et al., Transverse energy production and charged-particle multiplicity at midrapidity in various systems from $\sqrt{s_{NN}} =$ 7.7 to 200 GeV, Phys. Rev. C 93 (2) (2016) 024901, arXiv:1509.06727 [nucl-ex].

[16] ALICE Collaboration, J. Adam, et al., Measurement of transverse energy at midrapidity in Pb–Pb collisions at $\sqrt{s_{\rm NN}} = 2.76$ TeV, Phys. Rev. C 94 (3) (2016) 034903, arXiv:1603.04775 [nucl-ex].

[17] ALICE Collaboration, J. Adam, et al., Centrality dependence of pion freeze-out radii in Pb–Pb collisions at $\sqrt{s_{\rm NN}} = 2.76$ TeV, Phys. Rev. C 93 (2) (2016) 024905, arXiv:1507.06842 [nucl-ex].

[18] ALICE Collaboration Collaboration, Centrality determination using the Glauber model in Xe–Xe collisions at $\sqrt{s_{\rm NN}} = 5.44$ TeV, https://cds.cern.ch/record/2315401.

[19] ALICE Collaboration, S. Acharya, et al., Centrality and pseudorapidity dependence of the charged-particle multiplicity density in Xe–Xe collisions at $\sqrt{s_{\rm NN}} = 5.44$ TeV, arXiv:1805.04432 [nucl-ex].

[20] PHOBOS Collaboration, B. Alver, et al., System size and centrality dependence of charged hadron transverse momentum spectra in Au + Au and Cu + Cu collisions at $s(NN)**(1/2) = 62.4$-GeV and 200-GeV, Phys. Rev. Lett. 96 (2006) 212301, arXiv:nucl-ex/0512016 [nucl-ex].

[21] J. Bjorken, Energy Loss of Energetic Partons in Quark–Gluon Plasma: Possible Extinction of High $p_{\rm T}$ Jets in Hadron–Hadron Collisions, Tech. Rep. FERMILAB-PUB-82-059-T, Fermilab, 1982, http://lss.fnal.gov/archive/preprint/fermilab-pub-82-059-t.shtml.

[22] D. d'Enterria, Jet quenching, Landolt–Börnstein I/23, arXiv:0902.2011 [nucl-ex], 2010.

[23] A. Ortiz, O. Vázquez, Energy density and path-length dependence of the fractional momentum loss in heavy-ion collisions at $\sqrt{s_{\rm NN}}$ from 62.4 to 5020 GeV, Phys. Rev. C 97 (1) (2018) 014910, arXiv:1708.07571 [hep-ph].

[24] C. Loizides, J. Kamin, D. d'Enterria, Precision Monte Carlo Glauber predictions at present and future nuclear colliders, arXiv:1710.07098 [nucl-ex].

[25] CMS Collaboration, V. Khachatryan, et al., Charged-particle nuclear modification factors in PbPb and pPb collisions at $\sqrt{s_{\rm NN}} = 5.02$ TeV, J. High Energy Phys. 04 (2017) 039, arXiv:1611.01664 [nucl-ex].

[26] H.D. Vries, C.D. Jager, C.D. Vries, Nuclear charge-density-distribution parameters from elastic electron scattering, At. Data Nucl. Data Tables 36 (1987) 495–536, http://www.sciencedirect.com/science/article/pii/0092640X87900131.

[27] ALICE Collaboration, K. Aamodt, et al., The ALICE experiment at the CERN LHC, J. Instrum. 3 (2008) S08002.

[28] ALICE Collaboration, K. Aamodt, et al., Alignment of the ALICE inner tracking system with cosmic-ray tracks, J. Instrum. 5 (2010) P03003, arXiv:1001.0502 [physics.ins-det].

[29] J. Alme, et al., The ALICE TPC, a large 3-dimensional tracking device with fast readout for ultra-high multiplicity events, Nucl. Instrum. Methods A 622 (2010) 316–367, arXiv:1001.1950 [physics.ins-det].

[30] ALICE Collaboration, J. Adam, et al., Centrality dependence of the charged-particle multiplicity density at midrapidity in Pb–Pb collisions at $\sqrt{s_{\rm NN}} =$ 5.02 TeV, Phys. Rev. Lett. 116 (2016) 222302, arXiv:1512.06104 [nucl-ex].

[31] ALICE Collaboration, S. Acharya, et al., The ALICE Definition of Primary Particles, Public Note ALICE-PUBLIC-2017-005, CERN, 2017, https://cds.cern.ch/record/2270008.

[32] X.-N. Wang, M. Gyulassy, HIJING: a Monte Carlo model for multiple jet production in p–p, p–A and A–A collisions, Phys. Rev. D 44 (1991) 3501–3516.

[33] R. Brun, F. Bruyant, F. Carminati, S. Giani, M. Maire, A. McPherson, G. Patrick, L. Urban, GEANT: Detector Description and Simulation Tool; Oct. 1994, CERN Program Library, Long Writeup W5013, CERN, Geneva, 1993, https://cds.cern.ch/record/1082634.
[34] ALICE Collaboration, J. Adam, et al., Enhanced production of multi-strange hadrons in high-multiplicity proton–proton collisions, Nat. Phys. 13 (2017) 535–539, arXiv:1606.07424 [nucl-ex].
[35] ALICE Collaboration, B. Abelev, et al., Centrality dependence of π, K, p production in Pb–Pb collisions at $\sqrt{s_{\rm NN}} = 2.76$ TeV, Phys. Rev. C 88 (2013) 044910, arXiv:1303.0737 [hep-ex].
[36] ALICE Collaboration, B. Abelev, et al., K^0_S and Λ production in Pb–Pb collisions at $\sqrt{s_{\rm NN}} = 2.76$ TeV, Phys. Rev. Lett. 111 (2013) 222301, arXiv:1307.5530 [nucl-ex].
[37] ALICE Collaboration, B. Abelev, et al., Production of charged pions, kaons and protons at large transverse momenta in pp and Pb–Pb collisions at $\sqrt{s_{\rm NN}} = 2.76$ TeV, Phys. Lett. B 736 (2014) 196–207, arXiv:1401.1250 [nucl-ex].
[38] ALICE Collaboration, B.B. Abelev, et al., Performance of the ALICE experiment at the CERN LHC, Int. J. Mod. Phys. A 29 (2014) 1430044, arXiv:1402.4476 [nucl-ex].
[39] ALICE Collaboration, B. Abelev, et al., Energy dependence of the transverse momentum distributions of charged particles in pp collisions measured by ALICE, Eur. Phys. J. C 73 (2013) 2662, arXiv:1307.1093 [nucl-ex].
[40] P. Skands, S. Carrazza, J. Rojo, Tuning PYTHIA 8.1: the Monash 2013 tune, Eur. Phys. J. C 74 (2014) 3024, arXiv:1404.5630 [hep-ph].
[41] PHENIX Collaboration, A. Adare, et al., Scaling properties of fractional momentum loss of high-p_T hadrons in nucleus–nucleus collisions at $\sqrt{s_{NN}}$ from 62.4 GeV to 2.76 TeV, Phys. Rev. C 93 (2) (2016) 024911, arXiv:1509.06735 [nucl-ex].
[42] C. Loizides, A. Morsch, Absence of jet quenching in peripheral nucleus–nucleus collisions, Phys. Lett. B 773 (2017) 408–411, arXiv:1705.08856 [nucl-ex].
[43] G. Giacalone, J. Noronha-Hostler, M. Luzum, J.-Y. Ollitrault, Hydrodynamic predictions for 5.44 TeV Xe + Xe collisions, Phys. Rev. C 97 (3) (2018) 034904, arXiv:1711.08499 [nucl-th].
[44] P.F. Kolb, P. Huovinen, U.W. Heinz, H. Heiselberg, Elliptic flow at SPS and RHIC: from kinetic transport to hydrodynamics, Phys. Lett. B 500 (2001) 232–240, arXiv:hep-ph/0012137 [hep-ph].
[45] CMS Collaboration, S. Chatrchyan, et al., Measurement of the pseudorapidity and centrality dependence of the transverse energy density in Pb–Pb collisions at $\sqrt{s_{\rm NN}} = 2.76$ TeV, Phys. Rev. Lett. 109 (Oct 2012) 152303, https://link.aps.org/doi/10.1103/PhysRevLett.109.152303.
[46] M. Djordjevic, D. Zigic, M. Djordjevic, J. Auvinen, How to test path-length dependence in energy loss mechanisms: analysis leading to a new observable, arXiv:1805.04030 [nucl-th], 2018.
[47] R. Hagedorn, Multiplicities, $p_{\rm T}$ distributions and the expected hadron $\rightarrow$ quark–gluon phase transition, Riv. Nuovo Cimento 6 (1983) 1–50.

ALICE Collaboration

S. Acharya [138], F.T.-. Acosta [22], D. Adamová [94], J. Adolfsson [81], M.M. Aggarwal [98], G. Aglieri Rinella [36], M. Agnello [33], N. Agrawal [49], Z. Ahammed [138], S.U. Ahn [77], S. Aiola [143], A. Akindinov [65], M. Al-Turany [104], S.N. Alam [138], D.S.D. Albuquerque [120], D. Aleksandrov [88], B. Alessandro [59], R. Alfaro Molina [73], Y. Ali [16], A. Alici [11,54,29], A. Alkin [3], J. Alme [24], T. Alt [70], L. Altenkamper [24], I. Altsybeev [137], C. Andrei [48], D. Andreou [36], H.A. Andrews [108], A. Andronic [141,104], M. Angeletti [36], V. Anguelov [102], C. Anson [17], T. Antičić [105], F. Antinori [57], P. Antonioli [54], R. Anwar [124], N. Apadula [80], L. Aphecetche [112], H. Appelshäuser [70], S. Arcelli [29], R. Arnaldi [59], O.W. Arnold [103,115], I.C. Arsene [23], M. Arslandok [102], B. Audurier [112], A. Augustinus [36], R. Averbeck [104], M.D. Azmi [18], A. Badalà [56], Y.W. Baek [61,42], S. Bagnasco [59], R. Bailhache [70], R. Bala [99], A. Baldisseri [134], M. Ball [44], R.C. Baral [86], A.M. Barbano [28], R. Barbera [30], F. Barile [53], L. Barioglio [28], G.G. Barnaföldi [142], L.S. Barnby [93], V. Barret [131], P. Bartalini [7], K. Barth [36], E. Bartsch [70], N. Bastid [131], S. Basu [140], G. Batigne [112], B. Batyunya [76], P.C. Batzing [23], J.L. Bazo Alba [109], I.G. Bearden [89], H. Beck [102], C. Bedda [64], N.K. Behera [61], I. Belikov [133], F. Bellini [36], H. Bello Martinez [2], R. Bellwied [124], L.G.E. Beltran [118], V. Belyaev [92], G. Bencedi [142], S. Beole [28], A. Bercuci [48], Y. Berdnikov [96], D. Berenyi [142], R.A. Bertens [127], D. Berzano [36,59], L. Betev [36], P.P. Bhaduri [138], A. Bhasin [99], I.R. Bhat [99], H. Bhatt [49], B. Bhattacharjee [43], J. Bhom [116], A. Bianchi [28], L. Bianchi [124], N. Bianchi [52], J. Bielčík [39], J. Bielčíková [94], A. Bilandzic [115,103], G. Biro [142], R. Biswas [4], S. Biswas [4], J.T. Blair [117], D. Blau [88], C. Blume [70], G. Boca [135], F. Bock [36], A. Bogdanov [92], L. Boldizsár [142], M. Bombara [40], G. Bonomi [136], M. Bonora [36], H. Borel [134], A. Borissov [20,141], M. Borri [126], E. Botta [28], C. Bourjau [89], L. Bratrud [70], P. Braun-Munzinger [104], M. Bregant [119], T.A. Broker [70], M. Broz [39], E.J. Brucken [45], E. Bruna [59], G.E. Bruno [36,35], D. Budnikov [106], H. Buesching [70], S. Bufalino [33], P. Buhler [111], P. Buncic [36], O. Busch [130], Z. Buthelezi [74], J.B. Butt [16], J.T. Buxton [19], J. Cabala [114], D. Caffarri [90], H. Caines [143], A. Caliva [104], E. Calvo Villar [109], R.S. Camacho [2], P. Camerini [27], A.A. Capon [111], F. Carena [36], W. Carena [36], F. Carnesecchi [29,11], J. Castillo Castellanos [134], A.J. Castro [127], E.A.R. Casula [55], C. Ceballos Sanchez [9], S. Chandra [138], B. Chang [125], W. Chang [7], S. Chapeland [36], M. Chartier [126], S. Chattopadhyay [138], S. Chattopadhyay [107], A. Chauvin [103,115], C. Cheshkov [132], B. Cheynis [132], V. Chibante Barroso [36], D.D. Chinellato [120], S. Cho [61], P. Chochula [36], T. Chowdhury [131], P. Christakoglou [90], C.H. Christensen [89], P. Christiansen [81], T. Chujo [130], S.U. Chung [20], C. Cicalo [55], L. Cifarelli [11,29], F. Cindolo [54], J. Cleymans [123], F. Colamaria [53], D. Colella [66,36,53], A. Collu [80], M. Colocci [29], M. Concas [59,i], G. Conesa Balbastre [79], Z. Conesa del Valle [62], J.G. Contreras [39], T.M. Cormier [95], Y. Corrales Morales [59], P. Cortese [34], M.R. Cosentino [121], F. Costa [36], S. Costanza [135], J. Crkovská [62], P. Crochet [131], E. Cuautle [71], L. Cunqueiro [141,95], T. Dahms [103,115], A. Dainese [57], M.C. Danisch [102], A. Danu [69], D. Das [107], I. Das [107], S. Das [4], A. Dash [86], S. Dash [49], S. De [50], A. De Caro [32], G. de Cataldo [53], C. de Conti [119], J. de Cuveland [41], A. De Falco [26], D. De Gruttola [11,32], N. De Marco [59], S. De Pasquale [32], R.D. De Souza [120], H.F. Degenhardt [119], A. Deisting [104,102], A. Deloff [85], S. Delsanto [28], C. Deplano [90], P. Dhankher [49],

D. Di Bari [35], A. Di Mauro [36], B. Di Ruzza [57], R.A. Diaz [9], T. Dietel [123], P. Dillenseger [70], Y. Ding [7], R. Divià [36], Ø. Djuvsland [24], A. Dobrin [36], D. Domenicis Gimenez [119], B. Dönigus [70], O. Dordic [23], L.V.R. Doremalen [64], A.K. Dubey [139], A. Dubla [104], L. Ducroux [132], S. Dudi [98], A.K. Duggal [98], M. Dukhishyam [86], P. Dupieux [131], R.J. Ehlers [143], D. Elia [53], E. Endress [109], H. Engel [75], E. Epple [143], B. Erazmus [112], F. Erhardt [97], M.R. Ersdal [24], B. Espagnon [62], G. Eulisse [36], J. Eum [20], D. Evans [108], S. Evdokimov [91], L. Fabbietti [103,115], M. Faggin [31], J. Faivre [79], A. Fantoni [52], M. Fasel [95], L. Feldkamp [141], A. Feliciello [59], G. Feofilov [137], A. Fernández Téllez [2], A. Ferretti [28], A. Festanti [31,36], V.J.G. Feuillard [102], J. Figiel [116], M.A.S. Figueredo [119], S. Filchagin [106], D. Finogeev [63], F.M. Fionda [24], G. Fiorenza [53], M. Floris [36], S. Foertsch [74], P. Foka [104], S. Fokin [88], E. Fragiacomo [60], A. Francescon [36], A. Francisco [112], U. Frankenfeld [104], G.G. Fronze [28], U. Fuchs [36], C. Furget [79], A. Furs [63], M. Fusco Girard [32], J.J. Gaardhøje [89], M. Gagliardi [28], A.M. Gago [109], K. Gajdosova [89], M. Gallio [28], C.D. Galvan [118], P. Ganoti [84], C. Garabatos [104], E. Garcia-Solis [12], K. Garg [30], C. Gargiulo [36], P. Gasik [115,103], E.F. Gauger [117], M.B. Gay Ducati [72], M. Germain [112], J. Ghosh [107], P. Ghosh [138], S.K. Ghosh [4], P. Gianotti [52], P. Giubellino [104,59], P. Giubilato [31], P. Glässel [102], D.M. Goméz Coral [73], A. Gomez Ramirez [75], V. Gonzalez [104], P. González-Zamora [2], S. Gorbunov [41], L. Görlich [116], S. Gotovac [37], V. Grabski [73], L.K. Graczykowski [139], K.L. Graham [108], L. Greiner [80], A. Grelli [64], C. Grigoras [36], V. Grigoriev [92], A. Grigoryan [1], S. Grigoryan [76], J.M. Gronefeld [104], F. Grosa [33], J.F. Grosse-Oetringhaus [36], R. Grosso [104], R. Guernane [79], B. Guerzoni [29], M. Guittiere [112], K. Gulbrandsen [89], T. Gunji [129], A. Gupta [99], R. Gupta [99], I.B. Guzman [2], R. Haake [36], M.K. Habib [104], C. Hadjidakis [62], H. Hamagaki [82], G. Hamar [142], J.C. Hamon [133], R. Hannigan [117], M.R. Haque [64], J.W. Harris [143], A. Harton [12], H. Hassan [79], D. Hatzifotiadou [54,11], S. Hayashi [129], S.T. Heckel [70], E. Hellbär [70], H. Helstrup [38], A. Herghelegiu [48], E.G. Hernandez [2], G. Herrera Corral [10], F. Herrmann [141], K.F. Hetland [38], T.E. Hilden [45], H. Hillemanns [36], C. Hills [126], B. Hippolyte [133], B. Hohlweger [103], D. Horak [39], S. Hornung [104], R. Hosokawa [130,79], P. Hristov [36], C. Huang [62], C. Hughes [127], P. Huhn [70], T.J. Humanic [19], H. Hushnud [107], N. Hussain [43], T. Hussain [18], D. Hutter [41], D.S. Hwang [21], J.P. Iddon [126], S.A. Iga Buitron [71], R. Ilkaev [106], M. Inaba [130], M. Ippolitov [88], M.S. Islam [107], M. Ivanov [104], V. Ivanov [96], V. Izucheev [91], B. Jacak [80], N. Jacazio [29], P.M. Jacobs [80], M.B. Jadhav [49], S. Jadlovska [114], J. Jadlovsky [114], S. Jaelani [64], C. Jahnke [119,115], M.J. Jakubowska [139], M.A. Janik [139], C. Jena [86], M. Jercic [97], R.T. Jimenez Bustamante [104], M. Jin [124], P.G. Jones [108], A. Jusko [108], P. Kalinak [66], A. Kalweit [36], J.H. Kang [144], V. Kaplin [92], S. Kar [7], A. Karasu Uysal [78], O. Karavichev [63], T. Karavicheva [63], P. Karczmarczyk [36], E. Karpechev [63], U. Kebschull [75], R. Keidel [47], D.L.D. Keijdener [64], M. Keil [36], B. Ketzer [44], Z. Khabanova [90], S. Khan [18], S.A. Khan [138], A. Khanzadeev [96], Y. Kharlov [91], A. Khatun [18], A. Khuntia [50], M.M. Kielbowicz [116], B. Kileng [38], B. Kim [130], D. Kim [144], D.J. Kim [125], E.J. Kim [14], H. Kim [144], J.S. Kim [42], J. Kim [102], M. Kim [61,102], S. Kim [21], T. Kim [144], T. Kim [144], S. Kirsch [41], I. Kisel [41], S. Kiselev [65], A. Kisiel [139], J.L. Klay [6], C. Klein [70], J. Klein [36,59], C. Klein-Bösing [141], S. Klewin [102], A. Kluge [36], M.L. Knichel [36], A.G. Knospe [124], C. Kobdaj [113], M. Kofarago [142], M.K. Köhler [102], T. Kollegger [104], N. Kondratyeva [92], E. Kondratyuk [91], A. Konevskikh [63], M. Konyushikhin [140], O. Kovalenko [85], V. Kovalenko [137], M. Kowalski [116], I. Králik [66], A. Kravčáková [40], L. Kreis [104], M. Krivda [66,108], F. Krizek [94], M. Krüger [70], E. Kryshen [96], M. Krzewicki [41], A.M. Kubera [19], V. Kučera [94,61], C. Kuhn [133], P.G. Kuijer [90], J. Kumar [49], L. Kumar [98], S. Kumar [49], S. Kundu [86], P. Kurashvili [85], A. Kurepin [63], A.B. Kurepin [63], A. Kuryakin [106], S. Kushpil [94], M.J. Kweon [61], Y. Kwon [144], S.L. La Pointe [41], P. La Rocca [30], Y.S. Lai [80], I. Lakomov [36], R. Langoy [122], K. Lapidus [143], C. Lara [75], A. Lardeux [23], P. Larionov [52], E. Laudi [36], R. Lavicka [39], R. Lea [27], L. Leardini [102], S. Lee [144], F. Lehas [90], S. Lehner [111], J. Lehrbach [41], R.C. Lemmon [93], E. Leogrande [64], I. León Monzón [118], P. Lévai [142], X. Li [13], X.L. Li [7], J. Lien [122], R. Lietava [108], B. Lim [20], S. Lindal [23], V. Lindenstruth [41], S.W. Lindsay [126], C. Lippmann [104], M.A. Lisa [19], V. Litichevskyi [45], A. Liu [80], H.M. Ljunggren [81], W.J. Llope [140], D.F. Lodato [64], V. Loginov [92], C. Loizides [80,95], P. Loncar [37], X. Lopez [131], E. López Torres [9], A. Lowe [142], P. Luettig [70], J.R. Luhder [141], M. Lunardon [31], G. Luparello [60], M. Lupi [36], A. Maevskaya [63], M. Mager [36], S.M. Mahmood [23], A. Maire [133], R.D. Majka [143], M. Malaev [96], Q.W. Malik [23], L. Malinina [76,ii], D. Mal'Kevich [65], P. Malzacher [104], A. Mamonov [106], V. Manko [88], F. Manso [131], V. Manzari [53], Y. Mao [7], M. Marchisone [74,128,132], J. Mareš [68], G.V. Margagliotti [27], A. Margotti [54], J. Margutti [64], A. Marín [104], P. Martinengo [36], M.I. Martínez [2], G. Martínez García [112], M. Martinez Pedreira [36], S. Masciocchi [104], M. Masera [28], A. Masoni [55], L. Massacrier [62], E. Masson [112], A. Mastroserio [53], A.M. Mathis [103,115], P.F.T. Matuoka [119], A. Matyja [127,116], C. Mayer [116], M. Mazzilli [35],

M.A. Mazzoni [58], F. Meddi [25], Y. Melikyan [92], A. Menchaca-Rocha [73], E. Meninno [32], J. Mercado Pérez [102], M. Meres [15], C.S. Meza [109], S. Mhlanga [123], Y. Miake [130], L. Micheletti [28], M.M. Mieskolainen [45], D.L. Mihaylov [103], K. Mikhaylov [65,76], A. Mischke [64], A.N. Mishra [71], D. Miśkowiec [104], J. Mitra [138], C.M. Mitu [69], N. Mohammadi [36], A.P. Mohanty [64], B. Mohanty [86], M. Mohisin Khan [18,iii], D.A. Moreira De Godoy [141], L.A.P. Moreno [2], S. Moretto [31], A. Morreale [112], A. Morsch [36], V. Muccifora [52], E. Mudnic [37], D. Mühlheim [141], S. Muhuri [138], M. Mukherjee [4], J.D. Mulligan [143], M.G. Munhoz [119], K. Münning [44], M.I.A. Munoz [80], R.H. Munzer [70], H. Murakami [129], S. Murray [74], L. Musa [36], J. Musinsky [66], C.J. Myers [124], J.W. Myrcha [139], B. Naik [49], R. Nair [85], B.K. Nandi [49], R. Nania [54,11], E. Nappi [53], A. Narayan [49], M.U. Naru [16], A.F. Nassirpour [81], H. Natal da Luz [119], C. Nattrass [127], S.R. Navarro [2], K. Nayak [86], R. Nayak [49], T.K. Nayak [138], S. Nazarenko [106], R.A. Negrao De Oliveira [70,36], L. Nellen [71], S.V. Nesbo [38], G. Neskovic [41], F. Ng [124], M. Nicassio [104], J. Niedziela [139,36], B.S. Nielsen [89], S. Nikolaev [88], S. Nikulin [88], V. Nikulin [96], F. Noferini [11,54], P. Nomokonov [76], G. Nooren [64], J.C.C. Noris [2], J. Norman [79], A. Nyanin [88], J. Nystrand [24], H. Oh [144], A. Ohlson [102], J. Oleniacz [139], A.C. Oliveira Da Silva [119], M.H. Oliver [143], J. Onderwaater [104], C. Oppedisano [59], R. Orava [45], M. Oravec [114], A. Ortiz Velasquez [71], A. Oskarsson [81], J. Otwinowski [116], K. Oyama [82], Y. Pachmayer [102], V. Pacik [89], D. Pagano [136], G. Paić [71], P. Palni [7], J. Pan [140], A.K. Pandey [49], S. Panebianco [134], V. Papikyan [1], P. Pareek [50], J. Park [61], J.E. Parkkila [125], S. Parmar [98], A. Passfeld [141], S.P. Pathak [124], R.N. Patra [138], B. Paul [59], H. Pei [7], T. Peitzmann [64], X. Peng [7], L.G. Pereira [72], H. Pereira Da Costa [134], D. Peresunko [88], E. Perez Lezama [70], V. Peskov [70], Y. Pestov [5], V. Petráček [39], M. Petrovici [48], C. Petta [30], R.P. Pezzi [72], S. Piano [60], M. Pikna [15], P. Pillot [112], L.O.D.L. Pimentel [89], O. Pinazza [54,36], L. Pinsky [124], S. Pisano [52], D.B. Piyarathna [124], M. Płoskoń [80], M. Planinic [97], F. Pliquett [70], J. Pluta [139], S. Pochybova [142], P.L.M. Podesta-Lerma [118], M.G. Poghosyan [95], B. Polichtchouk [91], N. Poljak [97], W. Poonsawat [113], A. Pop [48], H. Poppenborg [141], S. Porteboeuf-Houssais [131], V. Pozdniakov [76], S.K. Prasad [4], R. Preghenella [54], F. Prino [59], C.A. Pruneau [140], I. Pshenichnov [63], M. Puccio [28], V. Punin [106], J. Putschke [140], S. Raha [4], S. Rajput [99], J. Rak [125], A. Rakotozafindrabe [134], L. Ramello [34], F. Rami [133], R. Raniwala [100], S. Raniwala [100], S.S. Räsänen [45], B.T. Rascanu [70], V. Ratza [44], I. Ravasenga [33], K.F. Read [127,95], K. Redlich [85,iv], A. Rehman [24], P. Reichelt [70], F. Reidt [36], X. Ren [7], R. Renfordt [70], A. Reshetin [63], J.-P. Revol [11], K. Reygers [102], V. Riabov [96], T. Richert [64,81], M. Richter [23], P. Riedler [36], W. Riegler [36], F. Riggi [30], C. Ristea [69], S.P. Rode [50], M. Rodríguez Cahuantzi [2], K. Røed [23], R. Rogalev [91], E. Rogochaya [76], D. Rohr [36], D. Röhrich [24], P.S. Rokita [139], F. Ronchetti [52], E.D. Rosas [71], K. Roslon [139], P. Rosnet [131], A. Rossi [31], A. Rotondi [135], F. Roukoutakis [84], C. Roy [133], P. Roy [107], O.V. Rueda [71], R. Rui [27], B. Rumyantsev [76], A. Rustamov [87], E. Ryabinkin [88], Y. Ryabov [96], A. Rybicki [116], S. Saarinen [45], S. Sadhu [138], S. Sadovsky [91], K. Šafařík [36], S.K. Saha [138], B. Sahoo [49], P. Sahoo [50], R. Sahoo [50], S. Sahoo [67], P.K. Sahu [67], J. Saini [138], S. Sakai [130], M.A. Saleh [140], S. Sambyal [99], V. Samsonov [96,92], A. Sandoval [73], A. Sarkar [74], D. Sarkar [138], N. Sarkar [138], P. Sarma [43], M.H.P. Sas [64], E. Scapparone [54], F. Scarlassara [31], B. Schaefer [95], H.S. Scheid [70], C. Schiaua [48], R. Schicker [102], C. Schmidt [104], H.R. Schmidt [101], M.O. Schmidt [102], M. Schmidt [101], N.V. Schmidt [95,70], J. Schukraft [36], Y. Schutz [36,133], K. Schwarz [104], K. Schweda [104], G. Scioli [29], E. Scomparin [59], M. Šefčík [40], J.E. Seger [17], Y. Sekiguchi [129], D. Sekihata [46], I. Selyuzhenkov [104,92], K. Senosi [74], S. Senyukov [133], E. Serradilla [73], P. Sett [49], A. Sevcenco [69], A. Shabanov [63], A. Shabetai [112], R. Shahoyan [36], W. Shaikh [107], A. Shangaraev [91], A. Sharma [98], A. Sharma [99], M. Sharma [99], N. Sharma [98], A.I. Sheikh [138], K. Shigaki [46], M. Shimomura [83], S. Shirinkin [65], Q. Shou [110,7], K. Shtejer [28], Y. Sibiriak [88], S. Siddhanta [55], K.M. Sielewicz [36], T. Siemiarczuk [85], D. Silvermyr [81], G. Simatovic [90], G. Simonetti [36,103], R. Singaraju [138], R. Singh [86], R. Singh [99], V. Singhal [138], T. Sinha [107], B. Sitar [15], M. Sitta [34], T.B. Skaali [23], M. Slupecki [125], N. Smirnov [143], R.J.M. Snellings [64], T.W. Snellman [125], J. Song [20], F. Soramel [31], S. Sorensen [127], F. Sozzi [104], I. Sputowska [116], J. Stachel [102], I. Stan [69], P. Stankus [95], E. Stenlund [81], D. Stocco [112], M.M. Storetvedt [38], P. Strmen [15], A.A.P. Suaide [119], T. Sugitate [46], C. Suire [62], M. Suleymanov [16], M. Suljic [36,27], R. Sultanov [65], M. Šumbera [94], S. Sumowidagdo [51], K. Suzuki [111], S. Swain [67], A. Szabo [15], I. Szarka [15], U. Tabassam [16], J. Takahashi [120], G.J. Tambave [24], N. Tanaka [130], M. Tarhini [112], M. Tariq [18], M.G. Tarzila [48], A. Tauro [36], G. Tejeda Muñoz [2], A. Telesca [36], C. Terrevoli [31], B. Teyssier [132], D. Thakur [50], S. Thakur [138], D. Thomas [117], F. Thoresen [89], R. Tieulent [132], A. Tikhonov [63], A.R. Timmins [124], A. Toia [70], N. Topilskaya [63], M. Toppi [52], S.R. Torres [118], S. Tripathy [50], S. Trogolo [28], G. Trombetta [35], L. Tropp [40], V. Trubnikov [3], W.H. Trzaska [125], T.P. Trzcinski [139], B.A. Trzeciak [64], T. Tsuji [129], A. Tumkin [106], R. Turrisi [57], T.S. Tveter [23], K. Ullaland [24],

E.N. Umaka [124], A. Uras [132], G.L. Usai [26], A. Utrobicic [97], M. Vala [114], J.W. Van Hoorne [36], M. van Leeuwen [64], P. Vande Vyvre [36], D. Varga [142], A. Vargas [2], M. Vargyas [125], R. Varma [49], M. Vasileiou [84], A. Vasiliev [88], A. Vauthier [79], O. Vázquez Doce [103,115], V. Vechernin [137], A.M. Veen [64], E. Vercellin [28], S. Vergara Limón [2], L. Vermunt [64], R. Vernet [8], R. Vértesi [142], L. Vickovic [37], J. Viinikainen [125], Z. Vilakazi [128], O. Villalobos Baillie [108], A. Villatoro Tello [2], A. Vinogradov [88], T. Virgili [32], V. Vislavicius [81], A. Vodopyanov [76], M.A. Völkl [101], K. Voloshin [65], S.A. Voloshin [140], G. Volpe [35], B. von Haller [36], I. Vorobyev [115,103], D. Voscek [114], D. Vranic [104,36], J. Vrláková [40], B. Wagner [24], H. Wang [64], M. Wang [7], Y. Watanabe [130], M. Weber [111], S.G. Weber [104], A. Wegrzynek [36], D.F. Weiser [102], S.C. Wenzel [36], J.P. Wessels [141], U. Westerhoff [141], A.M. Whitehead [123], J. Wiechula [70], J. Wikne [23], G. Wilk [85], J. Wilkinson [54], G.A. Willems [141,36], M.C.S. Williams [54], E. Willsher [108], B. Windelband [102], W.E. Witt [127], R. Xu [7], S. Yalcin [78], K. Yamakawa [46], S. Yano [46], Z. Yin [7], H. Yokoyama [79,130], I.-K. Yoo [20], J.H. Yoon [61], V. Yurchenko [3], V. Zaccolo [59], A. Zaman [16], C. Zampolli [36], H.J.C. Zanoli [119], N. Zardoshti [108], A. Zarochentsev [137], P. Závada [68], N. Zaviyalov [106], H. Zbroszczyk [139], M. Zhalov [96], X. Zhang [7], Y. Zhang [7], Z. Zhang [7,131], C. Zhao [23], V. Zherebchevskii [137], N. Zhigareva [65], D. Zhou [7], Y. Zhou [89], Z. Zhou [24], H. Zhu [7], J. Zhu [7], Y. Zhu [7], A. Zichichi [29,11], M.B. Zimmermann [36], G. Zinovjev [3], J. Zmeskal [111], S. Zou [7]

[1] *A.I. Alikhanyan National Science Laboratory (Yerevan Physics Institute) Foundation, Yerevan, Armenia*
[2] *Benemérita Universidad Autónoma de Puebla, Puebla, Mexico*
[3] *Bogolyubov Institute for Theoretical Physics, National Academy of Sciences of Ukraine, Kiev, Ukraine*
[4] *Bose Institute, Department of Physics and Centre for Astroparticle Physics and Space Science (CAPSS), Kolkata, India*
[5] *Budker Institute for Nuclear Physics, Novosibirsk, Russia*
[6] *California Polytechnic State University, San Luis Obispo, CA, United States*
[7] *Central China Normal University, Wuhan, China*
[8] *Centre de Calcul de l'IN2P3, Villeurbanne, Lyon, France*
[9] *Centro de Aplicaciones Tecnológicas y Desarrollo Nuclear (CEADEN), Havana, Cuba*
[10] *Centro de Investigación y de Estudios Avanzados (CINVESTAV), Mexico City and Mérida, Mexico*
[11] *Centro Fermi – Museo Storico della Fisica e Centro Studi e Ricerche "Enrico Fermi", Rome, Italy*
[12] *Chicago State University, Chicago, IL, United States*
[13] *China Institute of Atomic Energy, Beijing, China*
[14] *Chonbuk National University, Jeonju, Republic of Korea*
[15] *Comenius University Bratislava, Faculty of Mathematics, Physics and Informatics, Bratislava, Slovakia*
[16] *COMSATS Institute of Information Technology (CIIT), Islamabad, Pakistan*
[17] *Creighton University, Omaha, NE, United States*
[18] *Department of Physics, Aligarh Muslim University, Aligarh, India*
[19] *Department of Physics, Ohio State University, Columbus, OH, United States*
[20] *Department of Physics, Pusan National University, Pusan, Republic of Korea*
[21] *Department of Physics, Sejong University, Seoul, Republic of Korea*
[22] *Department of Physics, University of California, Berkeley, CA, United States*
[23] *Department of Physics, University of Oslo, Oslo, Norway*
[24] *Department of Physics and Technology, University of Bergen, Bergen, Norway*
[25] *Dipartimento di Fisica dell'Università 'La Sapienza' and Sezione INFN, Rome, Italy*
[26] *Dipartimento di Fisica dell'Università and Sezione INFN, Cagliari, Italy*
[27] *Dipartimento di Fisica dell'Università and Sezione INFN, Trieste, Italy*
[28] *Dipartimento di Fisica dell'Università and Sezione INFN, Turin, Italy*
[29] *Dipartimento di Fisica e Astronomia dell'Università and Sezione INFN, Bologna, Italy*
[30] *Dipartimento di Fisica e Astronomia dell'Università and Sezione INFN, Catania, Italy*
[31] *Dipartimento di Fisica e Astronomia dell'Università and Sezione INFN, Padova, Italy*
[32] *Dipartimento di Fisica 'E.R. Caianiello' dell'Università and Gruppo Collegato INFN, Salerno, Italy*
[33] *Dipartimento DISAT del Politecnico and Sezione INFN, Turin, Italy*
[34] *Dipartimento di Scienze e Innovazione Tecnologica dell'Università del Piemonte Orientale and INFN Sezione di Torino, Alessandria, Italy*
[35] *Dipartimento Interateneo di Fisica 'M. Merlin' and Sezione INFN, Bari, Italy*
[36] *European Organization for Nuclear Research (CERN), Geneva, Switzerland*
[37] *Faculty of Electrical Engineering, Mechanical Engineering and Naval Architecture, University of Split, Split, Croatia*
[38] *Faculty of Engineering and Science, Western Norway University of Applied Sciences, Bergen, Norway*
[39] *Faculty of Nuclear Sciences and Physical Engineering, Czech Technical University in Prague, Prague, Czech Republic*
[40] *Faculty of Science, P.J. Šafárik University, Košice, Slovakia*
[41] *Frankfurt Institute for Advanced Studies, Johann Wolfgang Goethe-Universität Frankfurt, Frankfurt, Germany*
[42] *Gangneung-Wonju National University, Gangneung, Republic of Korea*
[43] *Gauhati University, Department of Physics, Guwahati, India*
[44] *Helmholtz-Institut für Strahlen- und Kernphysik, Rheinische Friedrich-Wilhelms-Universität Bonn, Bonn, Germany*
[45] *Helsinki Institute of Physics (HIP), Helsinki, Finland*
[46] *Hiroshima University, Hiroshima, Japan*
[47] *Hochschule Worms, Zentrum für Technologietransfer und Telekommunikation (ZTT), Worms, Germany*
[48] *Horia Hulubei National Institute of Physics and Nuclear Engineering, Bucharest, Romania*
[49] *Indian Institute of Technology Bombay (IIT), Mumbai, India*
[50] *Indian Institute of Technology Indore, Indore, India*
[51] *Indonesian Institute of Sciences, Jakarta, Indonesia*
[52] *INFN, Laboratori Nazionali di Frascati, Frascati, Italy*
[53] *INFN, Sezione di Bari, Bari, Italy*
[54] *INFN, Sezione di Bologna, Bologna, Italy*
[55] *INFN, Sezione di Cagliari, Cagliari, Italy*
[56] *INFN, Sezione di Catania, Catania, Italy*

[57] INFN, Sezione di Padova, Padova, Italy
[58] INFN, Sezione di Roma, Rome, Italy
[59] INFN, Sezione di Torino, Turin, Italy
[60] INFN, Sezione di Trieste, Trieste, Italy
[61] Inha University, Incheon, Republic of Korea
[62] Institut de Physique Nucléaire d'Orsay (IPNO), Institut National de Physique Nucléaire et de Physique des Particules (IN2P3/CNRS), Université de Paris-Sud, Université Paris-Saclay, Orsay, France
[63] Institute for Nuclear Research, Academy of Sciences, Moscow, Russia
[64] Institute for Subatomic Physics, Utrecht University/Nikhef, Utrecht, Netherlands
[65] Institute for Theoretical and Experimental Physics, Moscow, Russia
[66] Institute of Experimental Physics, Slovak Academy of Sciences, Košice, Slovakia
[67] Institute of Physics, Bhubaneswar, India
[68] Institute of Physics of the Czech Academy of Sciences, Prague, Czech Republic
[69] Institute of Space Science (ISS), Bucharest, Romania
[70] Institut für Kernphysik, Johann Wolfgang Goethe-Universität Frankfurt, Frankfurt, Germany
[71] Instituto de Ciencias Nucleares, Universidad Nacional Autónoma de México, Mexico City, Mexico
[72] Instituto de Física, Universidade Federal do Rio Grande do Sul (UFRGS), Porto Alegre, Brazil
[73] Instituto de Física, Universidad Nacional Autónoma de México, Mexico City, Mexico
[74] iThemba LABS, National Research Foundation, Somerset West, South Africa
[75] Johann-Wolfgang-Goethe Universität Frankfurt Institut für Informatik, Fachbereich Informatik und Mathematik, Frankfurt, Germany
[76] Joint Institute for Nuclear Research (JINR), Dubna, Russia
[77] Korea Institute of Science and Technology Information, Daejeon, Republic of Korea
[78] KTO Karatay University, Konya, Turkey
[79] Laboratoire de Physique Subatomique et de Cosmologie, Université Grenoble-Alpes, CNRS-IN2P3, Grenoble, France
[80] Lawrence Berkeley National Laboratory, Berkeley, CA, United States
[81] Lund University Department of Physics, Division of Particle Physics, Lund, Sweden
[82] Nagasaki Institute of Applied Science, Nagasaki, Japan
[83] Nara Women's University (NWU), Nara, Japan
[84] National and Kapodistrian University of Athens, School of Science, Department of Physics, Athens, Greece
[85] National Centre for Nuclear Research, Warsaw, Poland
[86] National Institute of Science Education and Research, HBNI, Jatni, India
[87] National Nuclear Research Center, Baku, Azerbaijan
[88] National Research Centre Kurchatov Institute, Moscow, Russia
[89] Niels Bohr Institute, University of Copenhagen, Copenhagen, Denmark
[90] Nikhef, National institute for subatomic physics, Amsterdam, Netherlands
[91] NRC Kurchatov Institute IHEP, Protvino, Russia
[92] NRNU Moscow Engineering Physics Institute, Moscow, Russia
[93] Nuclear Physics Group, STFC Daresbury Laboratory, Daresbury, United Kingdom
[94] Nuclear Physics Institute of the Czech Academy of Sciences, Řež u Prahy, Czech Republic
[95] Oak Ridge National Laboratory, Oak Ridge, TN, United States
[96] Petersburg Nuclear Physics Institute, Gatchina, Russia
[97] Physics department, Faculty of science, University of Zagreb, Zagreb, Croatia
[98] Physics Department, Panjab University, Chandigarh, India
[99] Physics Department, University of Jammu, Jammu, India
[100] Physics Department, University of Rajasthan, Jaipur, India
[101] Physikalisches Institut, Eberhard-Karls-Universität Tübingen, Tübingen, Germany
[102] Physikalisches Institut, Ruprecht-Karls-Universität Heidelberg, Heidelberg, Germany
[103] Physik Department, Technische Universität München, Munich, Germany
[104] Research Division and ExtreMe Matter Institute EMMI, GSI Helmholtzzentrum für Schwerionenforschung GmbH, Darmstadt, Germany
[105] Rudjer Bošković Institute, Zagreb, Croatia
[106] Russian Federal Nuclear Center (VNIIEF), Sarov, Russia
[107] Saha Institute of Nuclear Physics, Kolkata, India
[108] School of Physics and Astronomy, University of Birmingham, Birmingham, United Kingdom
[109] Sección Física, Departamento de Ciencias, Pontificia Universidad Católica del Perú, Lima, Peru
[110] Shanghai Institute of Applied Physics, Shanghai, China
[111] Stefan Meyer Institut für Subatomare Physik (SMI), Vienna, Austria
[112] SUBATECH, IMT Atlantique, Université de Nantes, CNRS-IN2P3, Nantes, France
[113] Suranaree University of Technology, Nakhon Ratchasima, Thailand
[114] Technical University of Košice, Košice, Slovakia
[115] Technische Universität München, Excellence Cluster 'Universe', Munich, Germany
[116] The Henryk Niewodniczanski Institute of Nuclear Physics, Polish Academy of Sciences, Cracow, Poland
[117] The University of Texas at Austin, Austin, TX, United States
[118] Universidad Autónoma de Sinaloa, Culiacán, Mexico
[119] Universidade de São Paulo (USP), São Paulo, Brazil
[120] Universidade Estadual de Campinas (UNICAMP), Campinas, Brazil
[121] Universidade Federal do ABC, Santo Andre, Brazil
[122] University College of Southeast Norway, Tonsberg, Norway
[123] University of Cape Town, Cape Town, South Africa
[124] University of Houston, Houston, TX, United States
[125] University of Jyväskylä, Jyväskylä, Finland
[126] University of Liverpool, Department of Physics Oliver Lodge Laboratory, Liverpool, United Kingdom
[127] University of Tennessee, Knoxville, TN, United States
[128] University of the Witwatersrand, Johannesburg, South Africa
[129] University of Tokyo, Tokyo, Japan
[130] University of Tsukuba, Tsukuba, Japan
[131] Université Clermont Auvergne, CNRS/IN2P3, LPC, Clermont-Ferrand, France
[132] Université de Lyon, Université Lyon 1, CNRS/IN2P3, IPN-Lyon, Villeurbanne, Lyon, France
[133] Université de Strasbourg, CNRS, IPHC UMR 7178, F-67000, Strasbourg, France
[134] Université Paris-Saclay Centre d'Études de Saclay (CEA), IRFU, Department de Physique Nucléaire (DPhN), Saclay, France

[135] *Università degli Studi di Pavia, Pavia, Italy*
[136] *Università di Brescia, Brescia, Italy*
[137] *V. Fock Institute for Physics, St. Petersburg State University, St. Petersburg, Russia*
[138] *Variable Energy Cyclotron Centre, Kolkata, India*
[139] *Warsaw University of Technology, Warsaw, Poland*
[140] *Wayne State University, Detroit, MI, United States*
[141] *Westfälische Wilhelms-Universität Münster, Institut für Kernphysik, Münster, Germany*
[142] *Wigner Research Centre for Physics, Hungarian Academy of Sciences, Budapest, Hungary*
[143] *Yale University, New Haven, CT, United States*
[144] *Yonsei University, Seoul, Republic of Korea*

[i] Dipartimento DET del Politecnico di Torino, Turin, Italy.
[ii] M.V. Lomonosov Moscow State University, D.V. Skobeltsyn Institute of Nuclear, Physics, Moscow, Russia.
[iii] Department of Applied Physics, Aligarh Muslim University, Aligarh, India.
[iv] Institute of Theoretical Physics, University of Wroclaw, Poland.